ROBUST CONTROL DESIGN OF A HIGH PERFORMANCE FLEXIBLE ELECTRO-MECHANICAL SYSTEM

Yossi Chait

Associate Professor

Mechanical Engineering Department

University of Massachusetts

Amherst, MA 01003

Maarten Steinbuch

Member of Scientific Staff

Philips Research Laboratories

Prof. Holstlaan 4

5656 AA Eindhoven

The Netherlands

Myoung Soo Park

Director of Automated Products

Applied Light, Inc.

3640 Main St.

Springfield, MA 01107

1. ABSTRACT

This chapter considers the design and implementation of robust multivariable controllers applied to a Compact Disc mechanism. The design objective is to achieve good track-following and focusing performance in the presence of disturbances and structured uncertainty in the plant dynamics. In particular, the plant dynamics include lightly damped mechanical vibration modes. The robust performance problem has been solved in the μ-framework using the DK-iteration scheme and using a new, inversion-free, multivariable Quantitative Feedback Theory (QFT) technique. Implementation results of both designs in a Digital Signal Processor (DSP) environment are reported. The efficacy of the two design techniques as applied to this class of problems is discussed.

2. INTRODUCTION

A common problem encountered in control of large flexible space structures is the complexity of the dynamics, namely, a large number of lightly damped flexible modes in the systems. To meet stringent performance specifications, such structures must be actively controlled so to minimize the contribution of the flexible modes in the transient response. Control design requires knowledge of the plant dynamics, and the more accurate the model is, the better the achievable controlled performance is with lower costs. Analytic modeling of such structures is an inexact science, at the least, while obtaining models using extensive experimentation is often not feasible. Therefore, achieving robustness for parasitic dynamics becomes critical for successful design of high performance control systems.

In contrast to such systems, small actuator drives such as compact disc and hard disc drive mechanisms, are easy to access with experiments. In these high-volume electronics applications, the problem is to allow for tolerances during production, so as to decrease production costs. Hence, again we see the motivation to design robust performance controllers. Similarly to large flexible structures the dynamics includes flexible modes. Although model identification is more feasible, uncertainty modeling is still necessary to account for changes from product to product.

The research reported here focuses on all aspects of the robust control design for this class of systems including modeling of the dynamics, uncertainty representation, application of two leading control design techniques (μ-synthesis and QFT) and implementation.

In the next section we explain the basic operation of a CD-ROM mechanism. Section 4 discusses modeling aspects relevant for robust control design. The performance specifications are defined in Section 5. Details of two robust control designs using μ-synthesis and QFT techniques are presented in Sections 6-7, respectively. Section 8 provides details of the experimental setup and the implementation results of the two designs. Finally, conclusions and references are found in Sections 9-10, respectively.

3. THE COMPACT DISC MECHANISM

A Compact Disc player is an optical decoding device that reproduces high-quality audio from a digitally coded signal recorded as a spiral shaped track on a reflective disc [1]. Recently, apart from the audio application, other optical data systems (CD-ROM, Optical Data Drive) and combined audio/video and multi-media (CD-Interactive, MMCD) applications have emerged. An important research area for these applications is the possibility to increase the rotational frequency of the disc to obtain faster data readout and shorter access time. For higher rotational speeds, however, a higher servo bandwidth is required that approaches the resonance frequencies of bending and torsional modes of the CD-mechanism. Moreover, the system behavior varies from player to player due to the required manufacturing tolerances of CD players in mass-production, which explains the need for robustness of the controller.

The Compact Disc mechanism (Fig. 1) investigated in this study is composed of a turn-table DC-motor for the rotation of the disc, and a balanced radial arm for track-following. An optical element is mounted at the end of the radial arm. A diode located in this element generates a laser beam that passes through a series of optical lenses to reflect a spot on the information layer of the disc. An objective lens, suspended by two parallel leaf springs, can translate in a vertical direction for focusing action.

Figure 1: Schematic view of a rotating arm Compact Disc mechanism

Both the radial and the vertical (focus) position of the laser spot, relative to the track of the disc, must be controlled actively. To accomplish this, the controller uses position-error information provided by four photodiodes. As an input to the system, the controller generates the required control currents to the radial and focus actuator (which both are permanent-magnet/coil systems).

In Fig. 2, a block-diagram of the control system is shown. The difference between the radial and vertical track physical position and the actual spot position is detected by the optical pick-up; it generates a radial error signal erad and a focus error signal efoc via the optical gain Kopt. The controller K(s) feeds the system with the currents Irad and Ifoc. The matrix transfer function from control currents to spot position is indicated by H(s). Unique to this class of systems, only the position-error signals (after the optical gain) are available for measurement. Neither the true spot position nor the track position are available as signals.

Figure 2: Configuration of the control loop

In current systems the controller $K(s)$ is formed by two separate PID controllers [1,2], thus creating two single-input single-output (SISO) control loops. This is possible because the dynamic interaction between both loops is relatively low, especially from radial current to focus error. In the CD-ROM mechanism under consideration, the radial loop has a bandwidth of 500 Hz, while the bandwidth for the focus loop is 800 Hz. For more demanding applications, as discussed in Section 2, it becomes necessary to consider enhancement of the servo design.

4. MODELING

A measured frequency response of the CD-mechanism $G(s) = K_{opt}H(s)$ is given in Fig. 3 (magnitude only). At low frequencies, the rigid body mode of the radial arm and the lens-spring system (focus loop) can be easily recognized. It appears as a double integrator in the G_{11} and G_{22} elements of the matrix transfer function (MTF) G. At higher frequencies the measurement shows parasitic dynamics, especially in the radial direction. Experimental modal analyses and finite element calculations have revealed that these phenomena are due to mechanical resonances of the radial arm, mounting plate and disc (flexible bending and torsional modes).

Figure 3: Measured frequency response of the CD-mechanism (---) and of the identified 21st order model (- -)

In Fig. 4, a typical parasitic mode is shown, calculated with a finite element program.

Figure 4: Side view of the 4 kHz bending mode of the radial arm

Using frequency-domain-based system identification, each element of the frequency response has been fitted separately using an output error model structure with a least-square criterion [3]. Frequency dependent weighting functions have been used to improve the accuracy of the fit. The G_{21} element was especially difficult to fit because of the non-proper behavior in the frequency range of interest. In general, the high-frequency response of the off-diagonal elements is not very reliable since the coherence of the measurements was very low.

Combining the separate fits resulted in a 37th order multivariable state-space model. Using frequency weighted balanced reduction [4,5], this model was reduced to a 21st order model without significant loss in accuracy in the servo bandwidth. The frequency response of the model is shown in Fig. 3.

4.1. Uncertainty modeling

The most important variations in the CD dynamics from performance view point are:

i. unstructured difference between model and measurement,
ii. uncertain interaction,
iii. uncertain actuator gain, and
iv. uncertainty in the frequencies of the parasitic resonances.

The first uncertainty stems from the fact that our nominal model only is an approximation of the measured frequency response due to imperfect modeling. Further, a very high-order nominal model is undesirable in some robust control design techniques (e.g., μ-synthesis), since they yield controllers with the state dimension of the nominal model plus weighting functions. For that reason, our nominal model only describes the rigid body dynamics and the resonance modes that are most relevant for control design. Unmodeled high-frequency dynamics and the unstructured difference between model and measurement will be modeled as a complex valued additive perturbation Δa, bounded by a high-pass weighting function.

The remaining uncertainty sources (ii), (iii) and (iv), are all intended to reflect that manufacturing tolerances manifest themselves as variations in the frequency response from one CD mechanism to another. By so doing, we are able to appreciate the consequences of manufacturing tolerances on control design.

The uncertain interaction (ii) is modeled using two scalar output multiplicative parametric perturbations:

$$\begin{aligned} y &= (I + \Delta_o)Cx = Cx + w_o \\ w_o &= \Delta_o z_o \\ z_o &= Cx \end{aligned}$$

where

$$\Delta_o = \begin{bmatrix} 0 & w_{o1}\delta_{o1} \\ w_{o2}\delta_{o2} & 0 \end{bmatrix}$$

The scalar weights w_{o1} and w_{o2} are chosen equal to 0.1, implying 10% uncertainty. Note that these perturbations also perturb G_{11} and G_{22}. However, this effect is very small in comparison to the perturbation of the off-diagonal elements.

The interaction is assumed to be uncertain since our model describes $K_{opt}H(s)$. Hence, in control design we can only specify the required disturbance attenuation after K_{opt} (position-error e) and not at the disc itself (position-error ε). When K_{opt} is non-diagonal good disturbance attenuation at e does not imply good disturbance attenuation at the disc. We compensate for this by assuming uncertainty in the amount of interaction in the MTF G(s).

Dual to the uncertain interaction, the uncertain actuator gains (iii) are modeled as two scalar input multiplicative parametric perturbations:

$$
\begin{aligned}
\dot{x} &= Ax + B(I + \Delta_i)u = Ax + Bw_i \\
w_i &= \Delta_i z_i \\
z_i &= u
\end{aligned}
$$

where

$$\Delta_i = \begin{bmatrix} 0 & w_{i1}\delta_{i1} \\ w_{i2}\delta_{i2} & 0 \end{bmatrix}$$

The gain of each actuator is perturbed by 5%. With this value, also non-linear gain variations in the radial loop due to the rotating arm principle are accounted for, and further gain variations caused by variations in track shape, depth and slope of the pits on the disc and varying quality of the transparent substrate protecting the disc [3].

Finally, we consider variations in the undamped natural frequency of parasitic resonance modes (iv). From earlier robust control studies ([6]) it was learned that the resonances at 0.8, 1.6 and 4.3 kHz are especially important. To model these variations one could use additive or multiplicative frequency response embedding. However, this implies that the uncertainty is represented on an input-output basis rather than parametrically, which may result in an unnecessary design conservatism. In addition, high-order weighting functions may be required to arrive at an accurate bound on the frequency response. For this reason, we choose to model these frequency uncertainties as parametric perturbations in the nominal state-space model. To accomplish this we convert each second-order resonance mode in the A-matrix by a similarity transformation into the following real modal form [6]:

$$\begin{bmatrix} 0 & 1 \\ -\omega_0^2 & -2\beta\omega_0 \end{bmatrix}$$

The undamped natural frequency ω_0 of each mode appears as a parameter in the state-space model. The perturbation of the three resonance frequencies is carried out with the Parametric Uncertainty Modeling Toolbox [7]. The output of the Toolbox is a Linear Fractional Transformation description of the perturbed system

$$\begin{aligned} \dot{x} &= Ax + B_1 u + B_2 w_p \\ y &= C_1 x + D_{11} u + D_{12} w_p \\ z_p &= C_2 x + D_{21} u + D_{22} w_p \\ w_p &= \Delta_{par} z_p \end{aligned} \tag{1}$$

with a normalized, block diagonal, parametric perturbation structure

$$\Delta_{par} = \mathrm{diag}\left[\delta_1 I_1, \delta_2 I_2, \delta_3 I_3\right]$$

Each frequency perturbation involves a real-repeated perturbation block of multiplicity two. It is repeated because w0 appears quadratically in the A-matrix. The lower and upper bounds are chosen to be ±2.5% relative to their nominal values. In Fig. 5, the resulting set of models for $G_{11}(s)$ is shown.

Figure 5: The nominal model and the parametric uncertainty set of $G_{11}(s)$

5. PERFORMANCE SPECIFICATIONS

A major disturbance source for the controlled system are track-position irregularities. Within the standardization of CDs, a radial track deviation of 100 μm (eccentricity) and a track acceleration at scanning velocity of 0.4 $m/$ s2 are allowed, while in the vertical direction these values are 1 mm and 10 m/s^2, respectively. Apart from track position irregularities, a second important disturbance source are external mechanical shocks. Measurements show that during portable use disturbance signals occur at a frequency band concentrated between 5 and 150 Hz.

For the CD player to work properly, the maximum allowable position error is 0.1 μm in the radial direction, and 1 μm in the focus direction. In the frequency domain, these performance specifications can be translated into requirements on the shape of the (output) sensitivity function $S=(I+GK)^{-1}$. Note that track irregularities involve time-domain constraints on signals which are difficult to translate into frequency domain specifications. To obtain the required track disturbance attenuation, the magnitude of the sensitivity at the rotational frequency should be less than 10^{-3} in both the radial and the focus direction. Further, for frequencies up to 150 Hz the sensitivity should be sufficiently small to suppress the impact of mechanical shocks and higher harmonics of the disc eccentricity.

Because both QFT and μ-synthesis are frequency domain techniques, the above specifications must be appropriately defined. In μ-synthesis, we require that the singular values of the sensitivity function be bounded from above by the values shown in Fig. 6. In multivariable QFT, closed-loop specifications take on a different form. Specifically, we require that

$$\left|s_{ij}(j\omega)\right| \leq \eta_{ij}(\omega), \ \ i, j = 1,2, \ \ \text{for each} \ \ G \in \mathcal{G}$$

as shown Fig. 6. This implies that in multivariable QFT the degree of closed-loop interaction is explicitly defined.

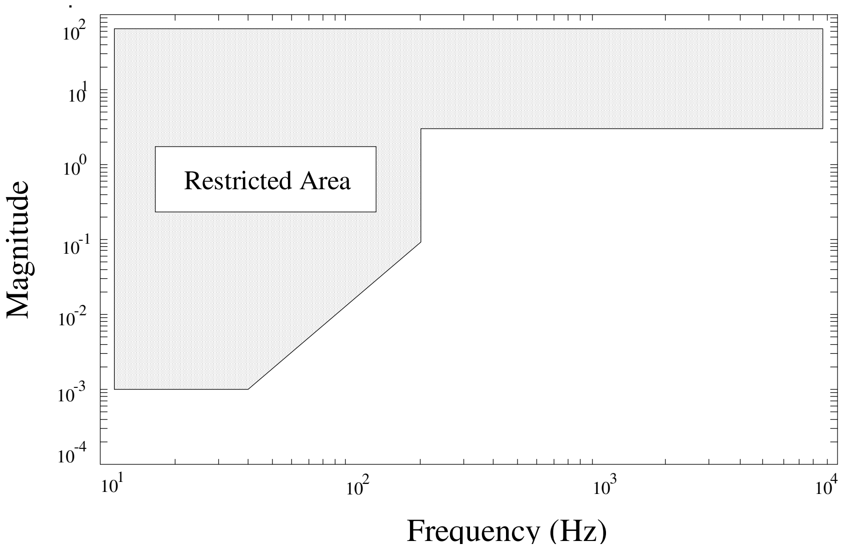

Figure 6: Sensitivity specifications

Satisfaction of the above requirements at increasing rotational speeds requires a similar increase in the servo bandwidth. As stated earlier, a higher bandwidth has implications on the robustness of the design against manufacturing tolerances. In addition, higher bandwidth implies higher power consumption (very critical in portable use), generation of audible noise by the actuators and bad playability of discs with surface scratches. Therefore, besides a disturbance rejection objective we are always striving towards a lowest possible servo bandwidth (<1 kHz).

In addition to these conflicting bandwidth requirements, the peak magnitude of the sensitivity function should be less than 3 to create sufficient phase margin in both loops. This is very important, since among several reasons the controller has to be discretized for implementation. Note that the invariance of the Bode sensitivity integral requires the trade-off between the sensitivity reduction and the phase margin specs.

6. μ-SYNTHESIS

6.1. Choice of Standard Plant

To begin with, the performance specification on S (sensitivity) can be combined with the robustness specifications associated with the transfer function KS accounting for the complex valued additive uncertainty Δa. The performance trade-offs are realized with a low-pass weighting function W1 on S, while imposing the weight W2 on KS reflects the size of the additive uncertainty and can also be used to force high roll-off at the input of the actuators. In this context, the objective to achieve robust performance implies [8] that for all stable, normalized perturbations Δ_a the closed loop is stable and

$$\left\| W_1 (I + [G + W_2 \Delta_a] K)^{-1} \right\|_\infty < 1$$

This objective is exactly equal to the requirement that

$$\mu_\Delta(\mathcal{F}_l(P_2, K)) < 1$$

with the interconnection

$$\mathcal{F}_l(P_2, K) = \begin{bmatrix} W_2 KS & W_2 KS \\ W_1 S & W_1 S \end{bmatrix} \tag{2}$$

where P2 is the standard plant (including the plant model and the weightings). The corresponding uncertainty structure is Δ=diag[Δ_a,Δ_p], where Δ_p is a 2×2 performance block. Note that the related H_∞ problem $\|\mathcal{F}_l(P_1, K)\|_\infty \leq 1$ where

$$\mathcal{F}_l(P_1, K) = \begin{bmatrix} W_2 KS \\ W_1 S \end{bmatrix} \tag{3}$$

a so-called *"S,KS"* design problem, yields robust *stability* and *only* nominal performance (although the original spec is robust performance). Standard H_∞ design on Eq. (2), i.e. $\|\mathcal{F}_l(P_2, K)\|_\infty \leq 1$, introduces a factor $\sqrt{2}$ compared to Eq. (3). Although it will achieve robust performance, it is clearly conservative since the known uncertainty structure is not accounted for. The μ-design for Eq. (2) will yield robust performance as required.

An alternative that we will use is to specify performance on the transfer function SG instead of S, reducing the resulting controller order by 4 [6]:

$$\mathcal{F}_l(P, K) = \begin{bmatrix} W_2 KS & W_2 KSG \\ W_1 S & W_1 SG \end{bmatrix} \tag{4}$$

The standard plant is shown in Fig. 7.

Figure 7: Standard plant for robust performance design

This design formulation has the additional advantage that it does not suffer from pole-zero cancellation as in the mixed sensitivity design formulations in Eq. (2).

6.2. Application to the CD Mechanism

Using the DK iteration scheme ([8,9]), μ-controllers are synthesized for several design problems of increasing degree of difficulty [10]. Starting with the robust performance problem in Eq. (4), the standard plant is augmented step by step with the parametric perturbations (ii), (iii) and (iv). In the final design problem we consider the complete uncertainty model, and the robust performance problem has 9 blocks:

$$\Delta = \mathrm{diag}[\,\delta_1 I_1, \delta_2 I_2, \delta_3 I_3, \delta_{i1}, \delta_{i2}, \delta_{o1}, \delta_{o2}, \Delta_a, \Delta_p]$$

In Fig. 8, the sensitivity frequency response is shown for the full problem μ-controller. For comparison, the result is also shown for two (i.e. radial and focus) PID controllers achieving 800 Hz bandwidth in both loops. Clearly, the μ-controller achieves superior disturbance rejection up to 150 Hz, has lower interaction and a lower sensitivity peaking value.

Figure 8: Nominal sensitivity with μ (---) and two PID controllers (- -)

The frequency responses of the controllers are shown in Fig. 9. As expected, the μ-controller has higher low-frequency gain and actively acts upon the resonance frequencies.

Figure 9: Frequency response of the μ-controller (---) and of two PID controllers (- - -)

6.3. Controller Reduction

The result of the μ-synthesis procedure for the full design problem is a controller with 83 states. This is primarily because of the dynamic D-scales necessary to account for the structure of the optimization problem. Of course, when the controller has to be experimentally validated this poses a problem. Digital implementation involves selection of the sampling frequency of the discretized controller [11,12]. Based on experience with previous implementations of SISO radial controllers (see [6]) and on the location of the fastest poles in the multivariable μ-controller (8 kHz), a frequency of 40 kHz was selected. However, the DSP environment limited the order of the controller that could be implemented to 8 at this sampling frequency. Controllers with high order would lead to an overload of the DSP. This indicated a need for a dramatic controller order reduction, since there is a large gap between the practically allowable controller order (<9) and the 83rd controller order computed using the μ-synthesis methodology. This posed a difficulty since the order of these controllers cannot be reduced to 8 without appreciable degradation of the nominal and robust performance. To facilitate implementation of higher-order controllers we can either design with a sampling frequency below 40 kHz, or use more than one DSP system and keep the sampling frequency at 40 kHz.

In this research we chose the latter, for it is expected that the necessary reduction of the sampling frequency sufficient for implementation would destroy the achievable performance. We have chosen to use two DSP boards as hardware set-up (each one with one input and two outputs, so as to realize all four parts of the MIMO controller). The controller to be implemented had to be order reduced from 83 to 2x8=16. The first step in the reduction procedure involved open-loop balancing followed by truncation of the (nearly) unobservable and/or uncontrollable state coordinates. The result of this balanced truncation was a 53rd order controller denoted $K_{53}(s)$. Inspection of the open-loop frequency response did not show any differences compared to the full-order controller. At all frequencies the maximum singular value of the additive reduction error was a factor 1000 or more smaller than the minimum singular value of the full-order controller.

The second step in the reduction procedure involved frequency weighted closed-loop balanced reduction of $K_{53}(s)$ as developed in [4,5]. We first briefly discuss below the frequency weighted closed-loop balanced reduction. Because the technique is completely dual for model and controller order reduction, we only discuss the controller reduction case.

The key idea is to use the same standard plant-controller interconnection structure used in H_∞ or μ-controller designs given by Eq. (4), with identical weightings, but with the parametric perturbations left out (see Fig. 7).

In a state-space realization of $\mathcal{F}_l(P,K)$ the state vector can be divided into $x=[x_P;x_K]$ where x_P represents the state vector of the plant and the weightings and x_K represents the state of the controller. The design freedom offered in the choice of similarity transformation on K is exploited to find a closed-loop balanced $\boldsymbol{K}$ such that $\boldsymbol{P_K}=\boldsymbol{Q_K}=\mathrm{diag}[\sigma_{\boldsymbol{K}}]$ with $\boldsymbol{P_K}$ and $\boldsymbol{Q_K}$ being the lower right part (K-part) of the controllability Gramian and of the observability Gramian of $\mathcal{F}_l(P,K)$ respectively. The Hankel Singular Values (HSV) $\sigma_{\boldsymbol{K}}$ are a measure for the contribution of the corresponding controller coordinates to the input-output behavior of the closed-loop configuration $\mathcal{F}_l(P,K)$, and by truncating $\boldsymbol{K}$ only the most important controller dynamics in terms of closed-loop performance are retained. This method is an extension of Enns' frequency weighted model reduction for closed-loop systems, and is applied interactively (the Weighted Order Reduction Toolbox (Wor-toolbox) [4]. This enables appropriate reduction despite the absence of an a priori error bound.

This Toolbox was used to reduce $K_{53}(s)$ as follows:

Step 1 : Write the open-loop controller $K_{53}(s)$ as two single-input two-output parts

$$K_{53}(s) = \begin{bmatrix} K_{53}^{1}(s) & K_{53}^{2}(s) \end{bmatrix} = C_K(sI - A_K)^{-1} \begin{bmatrix} B_K^{1} & B_K^{2} \end{bmatrix} \tag{5}$$

in which $K_{53}^{i}(s)$, i=1,2 is a 2 x1 MTF (columns of $K_{53}(s)$).

Step 2 : Construct the closed-loop configuration of Fig. 10 in which the output vector is split into the radial and focus output. The standard plant $P(s)$ is fed back with both columns $K_{53}^{1}(s)$ and $K_{53}^{2}(s)$ of the controller.

Figure 10: The closed-loop configuration used in the first step of frequency weighted closed-loop balanced reduction

Regard $P(s)$ with $K_{53}^{2}(s)$ in the feedback loop as the new standard plant $P^{1}(s)$ that has to be controlled by $K_{53}^{1}(s)$. In this closed-loop setting, reduce the order of $K_{53}^{1}(s)$ using the frequency weighted closed-loop balanced reduction technique.

Since the $K_{53}^{1}(s)$-realization $C_K(sI - A_K)^{-1}B_K$ has smaller controllability measures than the $K_{53}(s)$-realization of Eq. (5), there may be a possibility for a larger order reduction. Eventually, $K_{53}^{1}(s)$ should be reduced to $K_{8}^{1}(s)$ since it is the maximum order that can be implemented in a single DSP system operating at 40 kHz sampling frequency.

Step 3 : Once $K_{53}^{1}(s)$ has been reduced to $K_{8}^{1}(s)$, we can construct the dual closed-loop configuration with $P^{2}(s)$ fed back with $K_{53}^{2}(s)$ (see Fig. 11), and reduce its order in this configuration. As before, $K_{53}^{2}(s)$ should be reduced to $K_{8}^{2}(s)$ for implementation on a single DSP system at a sampling frequency of 40 kHz.

Figure 11: The closed-loop configuration used in the second step of frequency weighted closed-loop balanced reduction

Note that in $P^{2}(s)$, the CD-mechanism model is fed back with the already reduced-order $K_{8}^{1}(s)$ and not with the full-order $K_{53}^{1}(s)$. With this approach, the reduction result of the second column $K_{53}^{2}(s)$ accounts for the effects of the reduction of the first column. Note that this is not the case if we reduce $K_{53}^{1}(s)$ and $K_{53}^{2}(s)$ separately using open-loop reduction techniques.

An alternative to the above mentioned procedure is the application of the dual reduction procedure based on splitting the input vector u, i.e. row-wise separation of $K(s)$. However, we were not able to improve the result in this case.

The open-loop frequency response of the full 83rd order μ-controller of the complete design and the 2x8 reduced order version K_{8+8} is shown in Fig. 12. The difference between the two is largest above 2 kHz. Furthermore the (2,1) element is much different.

Figure 12: Open loop frequency response of K_{83}(---) and K_{8+8} (- -)

6.4. Practical Aspects of μ-Designs

The most significant experiences and limitations with respect to the use of μ-synthesis for this problem are:

- Convergence of the DK iteration scheme was fast (most cases 2 steps). Although global convergence of the scheme can not be guaranteed, in our design the resulting μ-controller did not depend on the starting controller.
- The final μ-controllers are of high order (83 for the full problem), due to the dynamic D-scales associated with the perturbations. This means that attention must be devoted to efficient order reduction of the final controller.
- Straightforward inclusion of the frequency perturbations into the standard plant caused numerical problems due to bad conditioning of the associated D-scales. For that reason, initially constant D-scaling was applied to Eq. (1).
- The Toolbox used for control design [8] did not allow fitting of D-scales for repeated perturbations. Therefore, each repeated perturbation had to be replaced by two independent scalar perturbations. μ-analysis revealed that this did not affect the μ-bounds.
- Although most of the perturbations are real-valued by nature, the assumption in design that all perturbations are complex valued (and non-repeated) did not introduce much conservatism with respect to robust performance (see Fig. 13). Note that the peak value of μ over frequency is 1.75, meaning that robust performance has not been achieved. This is due to the severe performance weighting W_1.
- The most difficult aspect of design appeared to be the shaping of weighting functions such that a proper trade-off is obtained between the conflicting performance and robustness specifications. In μ-synthesis

the weighting functions are the “design knobs” available to the engineer. This also points out the importance of the modeling of disturbances and specifications.

- The frequency-range of interest (1 Hz to 10 kHz) in this application did cause numerical problems. The problem was resolved by applying internal balancing and time-scaling to the weighting functions and to the nominal model.

Figure 13: Complex (---) and real (- -) μ-bounds for the μ-controller on the standard plant including all perturbations

7. QFT DESIGN

7.1. Problem Formulation

In multivariable QFT, the design problem is rigorously broken into an n-step sequential process (n=2 in our design). At each sequential step, n SISO QFT problems are solved for the n closed-loop transfer functions in that loop. In this investigation, we have employed new multivariable QFT algorithms which do not involve plant inversion used in all other multivariable QFT techniques (e.g., [13]). A brief overview of the new algorithms is given below (for complete details see [14]).

The sensitivity MTF is given by $S=(I+GK)^{-1}=\{s_{ij}\}, i,j=1,\ldots,n$. The plant model G, an nxn MTF, is uncertain and belongs to the set G. The controller is diagonal, K=diag[k1,...,kn]. The control objective is to design a controller, K, that in addition to achieving robust stability, satisfies the performance specification

$$\left|s_{ij}(j\omega)\right| \le \eta_{ij}(\omega), i, j = 1,2,\ldots,n, \quad \text{for each} \quad G \in \mathcal{G}$$

In the sequential procedure, at each ith step we use relations for sij, j=1,...,n, which are given in terms of the SISO controller ki [14]

$$s_{ij} = \frac{\alpha_{ji}^{L_1^{(i-1)}} + \sum_{k=i+1}^{n} -s_{kj}\,\alpha_{ki}^{L_1^{(i-1)}}}{\alpha_{ii}^{L_1^{(i-1)}} + \det[\,L_1^{(i-1)}]\,k_i}, \quad i, j = 1,2,\ldots,n \tag{6}$$

where $\alpha_{ij}^{L_1^{(i-1)}}$ is cofactor of $L_1^{(i-1)}$ (see [14]). Using the triangle inequality we can eliminate the unknowns s_{kj} (the closed-loop relations of loops not yet designed). The idea is to represent loop interactions as disturbances. The disturbances are represented in terms of closed-loop SISO elements of loops yet to be designed. If we assume that there exists a solution to the design problem, then it possible to replace the unknown disturbance by its worst case magnitude.

The following are the standard n SISO QFT problems at the ith step

$$\left|s_{ij}\right| \leq \frac{\left|\alpha_{ji}^{L_1^{(i-1)}}\right| + \sum_{k=i+1}^{n} \eta_{kj} \left|\alpha_{ki}^{L_1^{(i-1)}}\right|}{\left|\alpha_{ii}^{L_1^{(i-1)}} + \det[\, L_1^{(i-1)}] k_i\right|} \leq \eta_{ij} \text{ , } j = 1,2,\ldots n, \text{ for each } G \in \mathcal{G} \quad (7)$$

The robust stability criterion for the sequential, direct method requires that (under certain assumptions) each $1 + g_{ii}^{i} k_i$ is robust. Note that after the ith loop has been designed, the known controller k_i is sequentially embedded into the algorithms. Specifically, if $G=\{ g_{ij}^{1} \}$, then at the ith loop design step the effective plant elements include all known controllers ($k_1,...,k_{i-1}$) and are given by

$$g_{ij}^{i} = g_{ij}^{1} - \sum_{k=1}^{i-1} \frac{g_{kj}^{k}\, g_{ik}^{k}\, k_k}{1 + g_{kk}^{k}\, k_k} \tag{8}$$

To summarize the multivariable QFT technique, at each step in the sequential procedure we design a SISO controller to satisfy n SISO performance problems and one SISO stability problem.

7.2. Application to the CD Mechanism

In QFT we compute performance bounds only within a finite bandwidth (defined from the specifications), in this case, [0,200] Hz. In addition, the constraint $|s_{ii}(\omega)| \leq 3$, $\omega \geq 0$, is used to generate stability margin constraints on each loop as follows

$$\left|1 + g_{ii}^{i} k_i\right| \geq \frac{1}{3}, \ \omega \geq 0, \ \text{for each} \quad G \in \mathcal{G} \tag{9}$$

The final requirements are that the nominal open-loop bandwidth in each loop should be kept below 1 kHz to avoid amplifying high frequency noises and audible responses of the actuators, and that the controller order be kept to a minimum.

Note that although the open-loop system is weakly coupled, the specifications are truly multivariable since precise off-diagonal response is prescribed.

As discussed earlier, on the basis of experience and physical reasoning the nominal plant was assigned two types of uncertainties. The first type, parametric, consists of ±2.5% (independent) variations about nominal values in each of the undamped natural frequencies of the vibration modes at 0.8, 1.6 and 4.3 kHz. The second type, non-parametric, is related to the off-diagonal responses, and is defined as

$$G = \begin{bmatrix} g_{11} & \varepsilon g_{22} + g_{12} \\ \varepsilon g_{11} + g_{21} & g_{22} \end{bmatrix}, \ \varepsilon \in [-0.1, 0.1]$$

Note that the g_{ij} terms above already include parametric uncertainties.

In multivariable QFT design, there are three questions that should be answered prior to an actual design:

1. Do we need to decouple the plant and/or reorder inputs/outputs?
2. What is the best sequential order of loop closure?
3. How to grid G to represent a parametric plant uncertainty model?

The open-loop plant is already weakly coupled and the order is already physically defined, hence the first question is naturally solved. Unfortunately, no general rules exists for solving the second question. However, in most cases, it is possible to define this sequence based on the relative degree of difficulty loosely defined from the plant frequency response and the specifications at each loop. In our problem, g_{11} and g_{22} have similar responses up to 1 kHz, and since they have identical stability and performance specifications at that range, we expect the corresponding QFT bounds to be near identical at that range. Between 1 and 10 kHz, however, the effect of the mechanical resonances is more pronounced in g_{11}, hence stability bounds for g_{11} will be more "demanding " than those for g_{22}. We concluded that the first loop should be closed first. For the final question, in our plant there are only 4 parameters, so a crude grid over the parameter space (three natural frequencies and the interaction factor) should be sufficient. We used 375 plant cases to represent the uncertainty.

The first design step involves the radial controller k_1 to satisfy robust stability and the robust sensitivity performance specifications. It is always recommended to first view the plant uncertainties in terms of templates, and those for g_{11}^1 are shown in Fig. 14 at ω=[62.8, 251.3, 1257, 3142, 5404, 10120, 26890 and 62830] rad/sec. Note that Fig. 14 shows significant phase and magnitude variations at the three uncertain resonance frequencies.

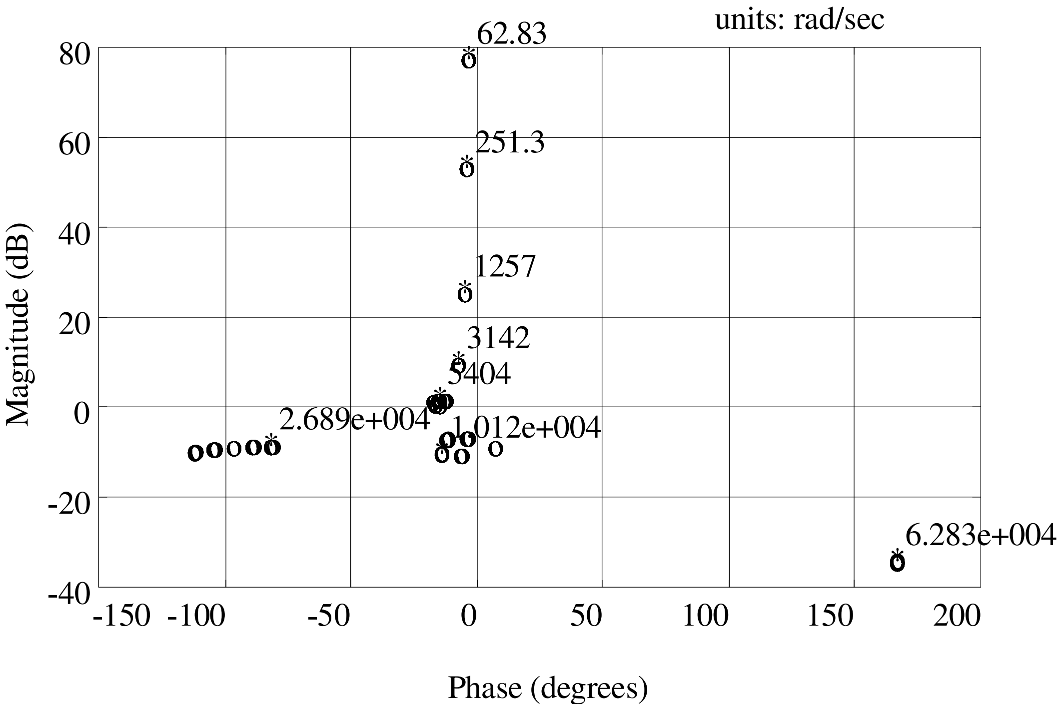

Figure 14: Templates of g_{11}^{1} used in the first step

To compute QFT stability bounds, we use the inequality defined by the margins problem in Eq. (9)

$$\left|1+\frac{g_{11}+\det[G]k_2}{1+g_{22}k_2}k_1\right|\geq\frac{1}{3}$$

Because k_2 is yet to be designed, we consider its extreme values, namely,

$$\begin{cases}\left|1+g_{11}k_1\right|\geq\dfrac{1}{3}\\[2ex]\left|1+\dfrac{\det[G]k_1}{g_{22}}\right|\geq\dfrac{1}{3}\end{cases}$$

To compute the sensitivity bounds invoke Eq. (6) to obtain

$$\begin{cases} |s_{11}(j\omega)| = \dfrac{1+\left|\dfrac{g_{12}\,s_{21}}{g_{22}}\right|}{\left|1+\dfrac{\det[G]k_1}{g_{22}}\right|} \le \dfrac{1+\left|\dfrac{g_{12}\,\eta_{21}}{g_{22}}\right|}{\left|1+\dfrac{\det[G]k_1}{g_{22}}\right|} \le \eta_{11}(\omega) \\ \\ |s_{12}(j\omega)| = \dfrac{\left|-\dfrac{g_{12}}{g_{22}}\right| + \left|\dfrac{g_{12}\,s_{22}}{g_{22}}\right|}{\left|1+\dfrac{\det[G]k_1}{g_{22}}\right|} \le \dfrac{\left|-\dfrac{k_{12}}{k_{22}}\right| + \left|\dfrac{g_{12}\,\eta_{22}}{g_{22}}\right|}{\left|1+\dfrac{\det[G]k_1}{g_{22}}\right|} \le \eta_{12}(\omega) \end{cases}$$

Robust stability bounds and robust sensitivity bounds were computed using slightly modified functions from the QFT Toolbox for MATLAB [15]. These bounds and the synthesized nominal loop are shown on the Nichols chart in Fig. 14.

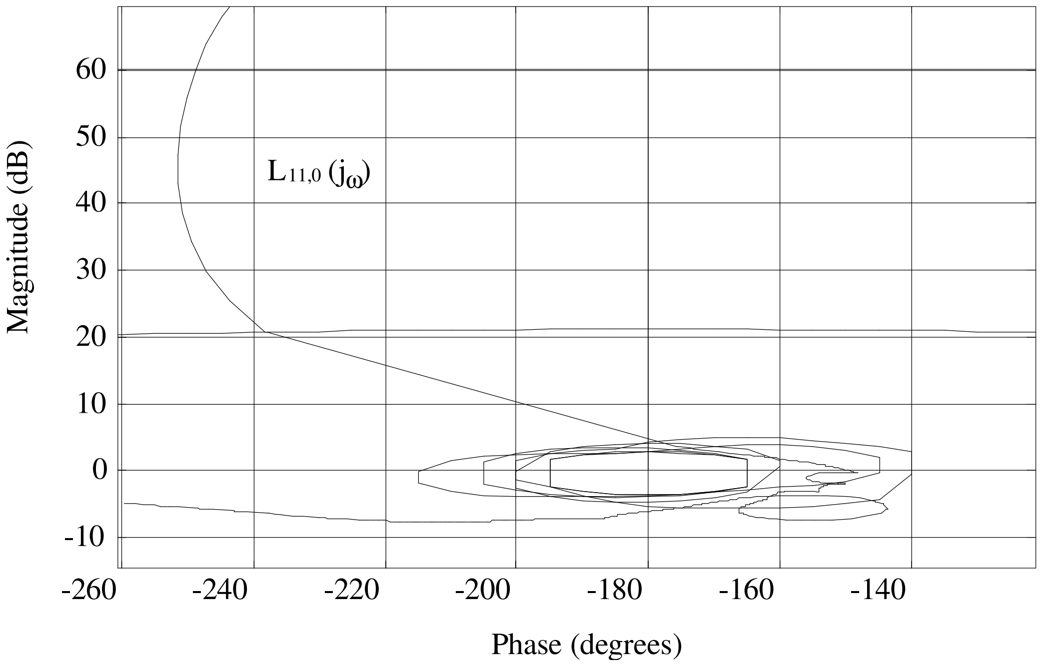

Figure 15: QFT bounds and nominal design $L_{11,0}(s)$ in the first design step

Note that $L_{11,0}(s)=g_{11,0}(s)k_1(s)$ where $g_{11,0}(s)$ is the nominal plant. The controller is given by (rounded off)

$$k_1 = \frac{1.33x10^{10}(s^2 + 2.8x10^3 s + 4.6x10^6)(s + 12.1)}{(s + 2.9x10^5)(s^2 + 2.6x10^4 s + 3.8x10^8)(s + 96)(s + 1)}$$

The second design step is to design k_2 to satisfy the robust stability and the robust performance specification while taking into account the known k_1. The plant used in the second design step, g_{22}^2, is defined by Eq. (8)

$$g_{22}^2 = g_{22} - \frac{g_{12}\,g_{21}k_1}{1 + g_{11}k_1}$$

and its templates are shown in Fig. 16. Note that due to the interaction, the templates of g_{22}^2 exhibit larger variations around the three uncertain natural frequencies compared with the templates g_{22} alone. Plant g_{22}^2 indeed is the plant seen by the controller to be designed.

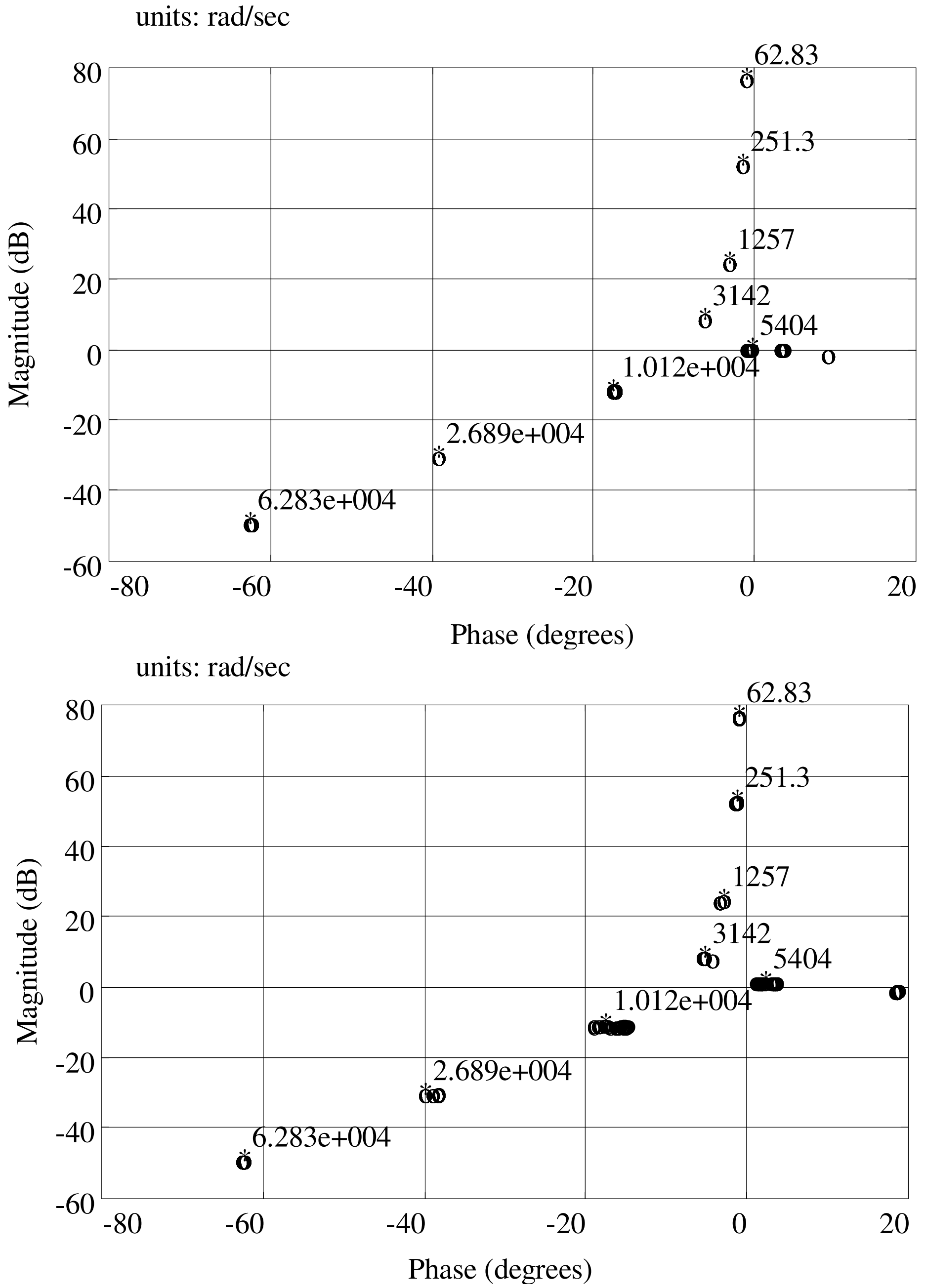

Figure 16: Templates of g_{22} (top) and g_{22}^{2} (bottom) used in the second step

Robust stability bounds are computed from Eq. (9)

$$\begin{cases} \left| 1+\dfrac{g_{22} + \det[G]k_1}{1+g_{11}k_1} k_2 \right| \geq \dfrac{1}{3} \\ \left| 1+\dfrac{g_{11} + \det[G]k_2}{1+g_{22}k_2} k_2 \right| \geq \dfrac{1}{3} \end{cases}$$

At this point, the only unknown is g_2. Sensitivity bounds are computed from Eq. (8)

$$\begin{cases} \left| s_{21}(j\omega) \right| = \left| \dfrac{\dfrac{-g_{21}k_1}{1+g_{11}k_1}}{1+\dfrac{g_{22}+\det[G]k_1}{1+g_{11}k_1} k_2} \right| \leq \eta_{21}(\omega) \\ \left| s_{22}(j\omega) \right| \leq \left| \dfrac{1}{1+\dfrac{g_{22}+\det[G]]k_1}{1+g_{11}k_1} k_2} \right| \leq \eta_{22}(\omega) \end{cases}$$

The robust stability bounds, robust sensitivity bounds and the synthesized nominal loop are shown on the Nichols chart in Fig. 17.

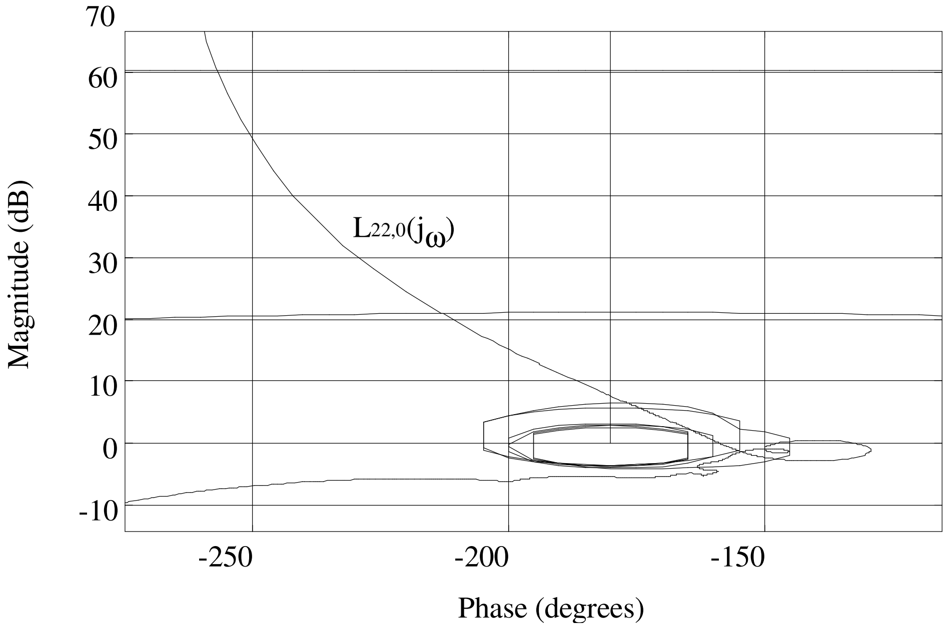

Figure 17: QFT bounds and nominal design $L_{22,0}(s)$ in the second step

Note that the nominal loop in the second design step is $L_{22,0}(s) = g^2_{22,0} k_1(s)$ where

$$g^2_{22,0} = g^2_{22} - \frac{g_{12,0} g_{21,0} k_1}{1 + g_{11,0} k_1}$$

The controller is given by (rounded off)

$$k_2 = \frac{2.9x10^4 (s + 2713.2)(s + 1622.2)}{(s^2 + 6.4x10^3 s + 2.9x10^8)(s + 1)}$$

As expected, the robust stability bounds in the second loop are less "demanding" compared with those obtained in the first loop. Specifically, in the crossover frequency range, the first nominal loop is required to maintain less phase lag compared with the demand on the second nominal loop.

7.3. Practical Aspects of Multivariable QFT Designs

The most significant experiences and limitations with respect to the use of multivariable QFT for this problem are as follows.

- Parametric uncertain plant models, such as the model used for our CD mechanism, must be converted into plant templates. Forming a grid in the parameter space with less than 100 points is a reasonable approach for plants with at most 2-3 uncertain parameters. However, the variations in the natural frequencies of the lightly damped modes require use of a finer grid. However, too many template points (say >1000) will slow down numerical computation of QFT bounds. One alternative, used here, was to study the relation between the grid and the resulting templates. The goal is to remove any points in the parameter space that correspond to interior plant template points. It was found out that a grid of 5 cases for each natural frequency and a grid of 3 for the off-diagonal gain is a minimum grid. This relatively course grid required careful consideration of the resulting bounds during loop shaping (i.e., avoidance of bounds).
- Manual loop shaping of k_1 was not a trivial task due to the location of nonminimum phase zero relative to the servo bandwidth. It required familiarity with conditionally stable loops and the concept of "phase lag maximization". It was found that controllers designed by other techniques (e.g., μ) can be effectively used to both study their general response as an initial design or fine-tuning within the QFT environment.
- It is yet to be established that an off-diagonal controller can result in an improved design in our problem, hence, use of a diagonal controller may

be justified. However, the QFT technique does not “provide ” general instructions to the designer as to how to exploit the inherent interaction in the plant in order to improve closed-loop performance (our present research focuses on this issue).

8. IMPLEMENTATION RESULTS

The actual implementation of the controllers in the DSP systems has been carried out with the dSPACE Cit-Pro software [11]. Most problems occurring when implementing controllers involve scaling inputs and outputs to obtain the appropriate signal levels and to ensure that the resolution of the DSP is optimally used. These problems can be solved in a user-friendly manner using the dSPACE software. The two DSP systems used were: a TMS320C30 16 bit processor with floating point arithmetic and a TMS320C25 16 bit processor with fixed point arithmetic. The Analog Digital Converters (ADC) are also 16 bit and have a conversion time of 5 μs. The maximum input voltage is ±10 V. The Digital Analog Converters (DAC) are 12 bit, have a conversion time of 3 μs and also operate within the range of ±10 V.

The first column $K_8^1(s) = [K_{11} \;\; K_{12}]^T$ has been implemented in the TMS320C30 processor at a sampling frequency of 40 kHz. The dSPACE software provides for:

- A ramp-invariant discretization,
- A modal transformation, and
- Generation of C code that can be downloaded to the DSP.

The second column $K_8^2(s) = [K_{21} \;\; K_{22}]^T$ was implemented on the TMS320C25 processor. Since this processor has fixed point arithmetic, scaling is more involved [12]. With the dSPACE software the following steps have been carried out:

- A ramp-invariant discretization,
- A modal transformation,
- l_1 scaling for the non-integrator states,

- State scaling for the integrator states such that their contribution is at most 20%, and
- Generation of DSPL code that can be downloaded to the DSP.

For the TMS320C25, a discretization at a sampling frequency of 40 kHz appeared to be too high, since it resulted in a processor load of 115%. For that reason, the sampling frequency of this DSP has been lowered to 34 kHz, yielding a processor load of 98.6%.

The DSP systems have been connected to the experimental set up by means of two analog summing junctions that have especially been designed for this purpose (Fig. 18).

Figure 18: The connection of both DSP systems to the experimental set up

When the external 2 x8 µ-controller of the complete design is connected to the experimental set up, we can measure the achieved performance in terms of the frequency response of the sensitivity function. The measurements have been carried out using a Hewlett Packard 3562 Dynamic Signal Analyzer. Since this analyzer can measure only SISO frequency responses, each of the four elements of the sensitivity function must be determined separately.

The measurements are started each time at the same radial position on the disc. This position is chosen approximately half way the disc, since the model used for control design was identified at that location, and also the radial gain is most constant in this region. In Fig. 19 the measured and simulated frequency response of the sensitivity function are shown. The off-diagonal elements are not very reliable since the coherence during these measurements was very low.

Figure 19: Measured frequency response of the sensitivity function with μ-controller K_{8+8} (---) and simulated with K_{83} (- - -)

The nominal performance has been tested in terms of the possibility to increase the rotational frequency of the Compact Disc. It appeared possible to achieve an increase in speed of a factor 4.

The diagonal multivariable QFT controller was implemented using two DSP boards as done with the μ-controller. The discretization was done at a sampling rate of 27 kHz. The measured closed-loop sensitivity magnitudes are shown in Fig. 20.

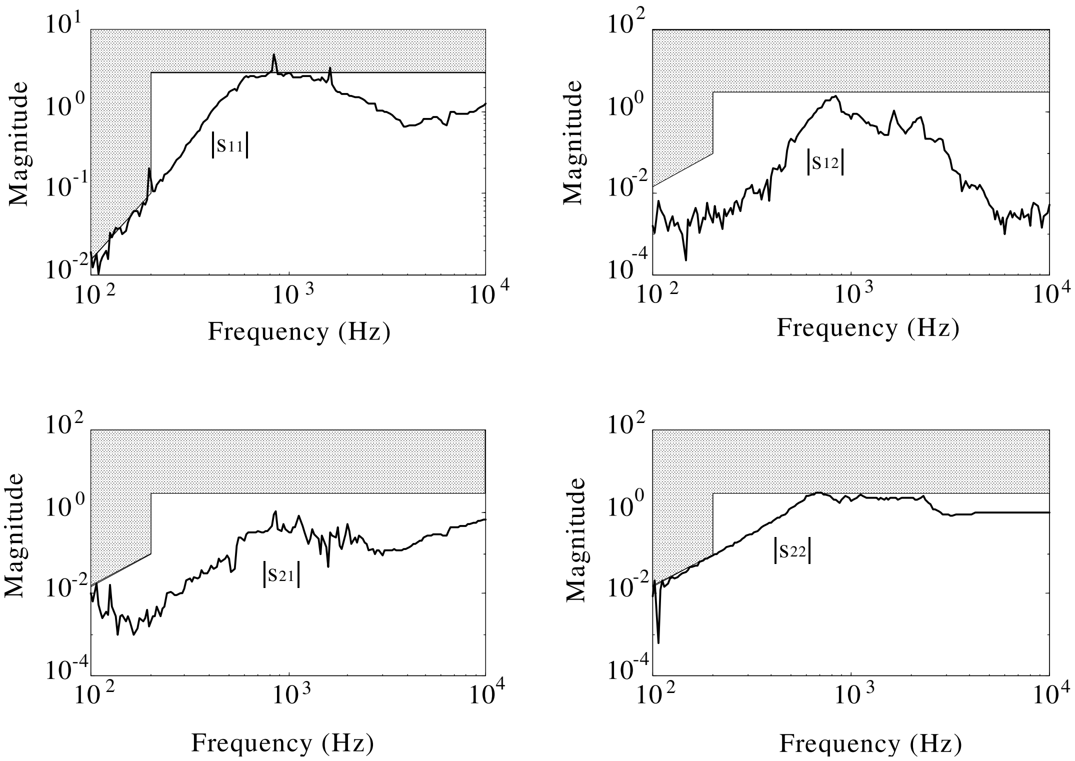

Figure 20: Measured frequency response magnitudes of the sensitivity functions with QFT controller

The observed peaks in $s_{11}(j\omega)$, especially in the 800-2000 Hz range, is attributed to identification errors in the nominal plant. A detailed comparison between the identified radial loop and the measured data around those peaks (Fig. 3) revealed that although the magnitudes matched well the phases were off by a few degrees. A SISO QFT design was subsequently carried out and implemented in the radial loop using the raw experimental frequency response data (since with QFT the designer can work directly with measured frequency response data). The new design did not exhibit such peaks [16].

9. CONCLUSIONS

In this paper multivariable QFT and μ-synthesis techniques have been applied to a Compact Disc player. The design objective was to achieve good track-following and focusing performance in the presence of disturbances and structured uncertainty in the lightly damped plant dynamics. Experimental results show that with use of the two design techniques, considerable improvement can be achieved in the track-following quality of disc drives. Such an improvement allows for a significant increase in the rotational frequency of the disc.

10. REFERENCES

1. G. Bouwhuis, et al., *Principles of Optical Disc Systems* (Adam Hilger Ltd., Bristol, UK, 1985).
2. W.M. Draijer, M. Steinbuch and O.H. Bosgra, *IFAC Automatica*, 28 (1992): .455-462.
3. R. Schrama, *Approximate Identification and Control Design*, PhD Thesis, (Delft Univ. Technology, The Netherlands, 1992).
4. P. Wortelboer, *Frequency Weighted Balanced Reduction of Closed-loop Mechanical Servo-systems: Theory and Tools*, PhD Thesis, (Delft Univ. Technology, The Netherlands, 1994).
5. P. Wortelboer, and O.H. Bosgra, *Procs. IEEE CDC*, (1992): 2848-2849.
6. M. Steinbuch, G. Schootstra and O.H. Bosgra, *Procs. IEEE CDC*, (1992): 2596-2600.
7. P. Lambrechts, J.C. Terlouw, S. Bennani and M. Steinbuch, *Procs. ACC*, (1993): 267-272.
8. G.J. Balas, J.C. Doyle, K. Glover, A.K. Packard and R. Smith, *μ-Analysis and Synthesis Toolbox,* (MUSYN Inc., Minneapolis, 1991).
9. J.C. Doyle, *Advances in Multivariable Control*, Lecture Notes of the ONR/Honeywell Workshop, (Honeywell, Minnesota, 1984).
10. P.J.M. Groos, M. Steinbuch and O.H. Bosgra, *Procs. 2nd European Control Conference*, (1993): 981-985.
11. dSPACE GmbH, *DSPCitPro software package*, Documentation of dSPACE (GmbH, Germany, 1989).
12. M. Steinbuch, G. Schootstra, and H.T. Goh*, IEEE Trans. on Control Systems Technology*, 2 (1994): 312-317.
13. I. Horowitz, *Int. J. Control*, 53 (1991): 255-291.

14. M.S. Park , *A New Approach to Multivariable Quantitative Feedback Theory* ," Ph.D. Thesis, (Univ. of Massachusetts, MA, 1994).
15. C. Borghesani, Y. Chait, and O. Yaniv, *The QFT Toolbox for MATLAB* , (The MathWorks, Inc., USA, 1995).
16. Y. Chait, M.S. Park, and M. Steinbuch, *J. Systems Engineering* , 4 (1994): 107-117.